

Diagnosing the possible chiral superconductivity in Sr_2RuO_4 and beyond using supercurrent

Hao-Tian Liu,^{1,2,3} Weipeng Chen,^{1,2,3} Jia-Xin Yin,⁴ Cai Liu,⁵ and Wen Huang^{1,2,3,*}

¹*Shenzhen Institute for Quantum Science and Engineering,
Southern University of Science and Technology, Shenzhen 518055, Guangdong, China*

²*International Quantum Academy, Shenzhen 518048, China*

³*Guangdong Provincial Key Laboratory of Quantum Science and Engineering,
Southern University of Science and Technology, Shenzhen 518055, China*

⁴*Department of Physics, Southern University of Science and Technology, Shenzhen, Guangdong, China*

⁵*College of Integrated Circuits and Optoelectronic Chips,
Shenzhen Technology University, Shenzhen 518118, Guangdong, China*

(Dated: August 29, 2023)

One approach to probe the still controversial superconductivity in Sr_2RuO_4 is to apply external perturbations that break the underlying tetragonal crystalline symmetry. Chiral $p_x + ip_y$ and $d_{xz} + id_{yz}$ states respond to such perturbations in ways that may help to distinguish them from other superconducting pairings. However, past experimental efforts along this line, using uniaxial strains and magnetic fields parallel to the RuO_2 plane, have not been able to reach unambiguous conclusion. In this study, we propose to diagnose the possible chiral superconducting order in Sr_2RuO_4 using an alternative tetragonal-symmetry-breaking perturbation — in-plane supercurrent. We study the superconducting phase diagram as a function of both temperature and the applied supercurrent. Supercurrent generically splits the transition of the two chiral order parameter components, and we show that the splitting can give rise to visible specific heat anomalies. Furthermore, supercurrent parallel and anti-parallel to the unidirectional propagation of the chiral edge modes impact the edge states in different manner. This difference manifests in tunneling spectrum, thereby providing an additional means to probe the chirality even when the related spontaneous edge current is vanishingly small. Finally, we discuss how supercurrent may help to identify other time-reversal symmetry breaking superconducting states. Our proposal applies to other candidate chiral superconductors.

I. INTRODUCTION

The Cooper pairing in chiral superconductors spontaneously breaks time-reversal symmetry, which can be detected by zero-field muon spin relaxation and optical polar Kerr effect measurements. Intrinsic chiral superconductors are hard to come by. Existing signatures consistent with chiral states have only been reported in a limited few materials, including Sr_2RuO_4 [1, 2], UPT_3 [3, 4], URu_2Si_2 [5, 6], although none of the above is unambiguously confirmed chiral superconductor.

Sr_2RuO_4 is among the most thoroughly studied candidate chiral superconductor. In the past three decades, much progress has been made towards unraveling the myth of its superconductivity. However, the exact nature of the Cooper pairing in this material remains hugely controversial [7–17]. In particular, while multiple early observations pointed to chiral $p_x + ip_y$ pairing [1, 2, 18–20], a number of recent key observations seem to defy a straightforward chiral p-wave interpretation [21, 22].

One approach to identify chiral p-wave pairing is to apply a perturbation that affects the p_x and p_y components of the superconducting order parameter in different manner [23]. For example, in-plane uniaxial strain breaks the tetragonal symmetry of Sr_2RuO_4 and may therefore lift

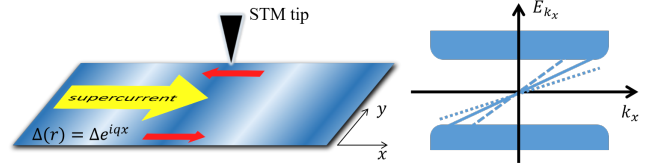


FIG. 1. Left: Sketch of a two-dimensional chiral superconductor in the presence of an injected supercurrent (yellow arrow). The red arrows indicate the flow of spontaneous edge current or the group velocity of chiral edge modes. The different size of the two red arrows reflects the unequal supercurrent-induced changes to the spontaneous edge current and chiral edge dispersion. Right: Sketch of the low-energy quasiparticle spectrum at one of the edges parallel to the x -direction. The in-gap chiral edge dispersion for cases without supercurrent, with left and right supercurrent are displayed as solid, dashed and dotted lines, respectively. Note the continuum spectrum in the presence of supercurrent is not sketched. The supercurrent-induced low-energy spectral variation at any boundary can be probed by tunneling spectroscopic techniques, such as STM and point contact.

the degeneracy between the two components [27]. However, the conclusion drawn from strain measurements is not conclusive. On the one hand, muon spin relaxation under strain indicates a splitting between an upper superconducting transition and a lower one breaking time-reversal symmetry [24]. On the other hand, dedicated thermodynamic study has failed to observe any

* huangw3@sustech.edu.cn

signature ascribable to two successive transitions [25, 26], while a number of other measurements did not reveal the expected linear cusp associated with the upper transition [27–29]. Apart from in-plane strain, similar symmetry breaking is also achieved with the application of in-plane magnetic field [30, 31]. Interestingly, once again no clear secondary transition has been observed in the most up-to-date specific heat experiment under in-plane fields [32].

Another analogous idea is to inject a supercurrent which can also lift the degeneracy of the two chiral components. In the past, the tunneling spectrum of a single-component superconductor subject to a supercurrent has been studied [33, 34]. In this work, we study the effect of in-plane d.c. supercurrent on a two-dimensional chiral p-wave superconductor. Generally speaking, the leading order impact of a supercurrent J is captured by the following terms in the free energy (assuming a charge neutral system),

$$(\alpha + a_x J^2)|\Delta_x|^2 + (\alpha + a_y J^2)|\Delta_y|^2. \quad (1)$$

Here, $\Delta_{x/y}$ denote the two chiral order parameter components, α and $a_{x/y}$ are coefficients that depend on microscopic details. Note that the absence of terms linear in J is because supercurrent flowing parallel and antiparallel to a specific direction should have the same effect on any individual order parameter component in the bulk. Hence, unlike the theoretically expected linear variation of the transition temperature with uniaxial strain, the critical temperature T_c should follow a quadratic dependence on small supercurrent.

We shall model the current-carrying state by considering Cooper pairings that exhibit finite center-of-mass momentum $2\mathbf{q}$, i.e. a Fulde-Ferrell state [35] (with supercurrent $J \propto \mathbf{q}$). By means of self-consistent mean-field Bogoliubov de-Gennes calculations, we then determine the phase diagram as a function of both \mathbf{q} and temperature. We further show that the splitting of the two chiral components will also manifest as two anomalies in specific heat.

Besides the bulk probe mentioned above, chiral edge modes and spontaneous edge current are another set of phenomena often associated with chiral superconductivity [36]. However, while the chiral edge modes are topologically protected, the edge current is not [37, 38]. The latter can be sensitive to microscopic details and disorder [37, 39–43], prompting an argument that the experimental null result on the edge current in Sr_2RuO_4 [44–46] can still be compatible with a chiral superconducting state. Hence edge current may not serve as an effective diagnosis of chiral superconductivity. In fact, to the best of our knowledge, there is not a single case where spontaneous edge current has been explicitly detected in candidate chiral superconductors. We propose in this study an alternative diagnosis by looking at the supercurrent-induced changes to the chiral edge modes: at any edge of a chiral superconductor, left and right supercurrents perturb the chiral edge dispersion differently, giving rise

to different corrections to the edge tunneling spectrum (see right panel of Fig. 1).

The rest of the paper is organized as follows. In Sec. II A we introduce the self-consistent mean-field formalism for studying the effects of supercurrent. The numerical results, including the q - T phase diagram, are presented in Sec. II B. Section II C demonstrates the supercurrent-induced splitting of the specific heat anomaly. In Sec. II D, we focus on the response of chiral edge modes to supercurrent and study the distinct changes to the edge tunneling spectrum in the presence of opposite supercurrents. Section III concludes the paper by discussing the identification of other time-reversal-symmetry-breaking (TRSB) superconducting states by means of applying a supercurrent.

II. FORMALISM AND RESULTS

A. Formalism

In the absence of supercurrent, Cooper pairing takes place between electrons with opposite momenta \mathbf{k} and $-\mathbf{k}$. A supercurrent state is described by Cooper pairings with a net center-of-mass momentum $2\mathbf{q}$, i.e. between electrons with momenta $\mathbf{k} + \mathbf{q}$ and $-\mathbf{k} + \mathbf{q}$. Equivalently, the superconducting order parameter acquires real-space phase modulation $\Delta \rightarrow \Delta e^{2i\mathbf{q}\cdot\mathbf{R}}$ [47], where \mathbf{R} is the center-of-mass position of the Cooper pair. Consider a simplified single-band spinless $p_x + ip_y$ model on a square lattice, an effective Hamiltonian then follows as:

$$\hat{H} = \sum_{\mathbf{k}} \xi_{\mathbf{k}} \hat{c}_{\mathbf{k}}^\dagger \hat{c}_{\mathbf{k}} + \sum_{\mathbf{k}, \mathbf{k}'} \tilde{U}_{\mathbf{k}, \mathbf{k}'} \hat{c}_{\mathbf{k}+\mathbf{q}}^\dagger \hat{c}_{-\mathbf{k}+\mathbf{q}}^\dagger \hat{c}_{-\mathbf{k}'+\mathbf{q}} \hat{c}_{\mathbf{k}'+\mathbf{q}}, \quad (2)$$

where $\xi_{\mathbf{k}} = 2t(\cos k_x + \cos k_y) - \mu$ is the electron dispersion in the normal state, t is the hopping amplitude, μ is the chemical potential, and $\tilde{U}_{\mathbf{k}, \mathbf{k}'}$ is the effective interaction in the p-wave Cooper channel. The effective interaction can be decomposed as $\tilde{U}_{\mathbf{k}, \mathbf{k}'} = \tilde{U}_{x, \mathbf{k}, \mathbf{k}'} + \tilde{U}_{y, \mathbf{k}, \mathbf{k}'}$, where the two terms on the right hand side are to generate p_x and p_y pairings respectively and each can be written in a separable form $\tilde{U}_{\alpha, \mathbf{k}, \mathbf{k}'} = -\tilde{U}_0 f_{\alpha, \mathbf{k}} f_{\alpha, \mathbf{k}'}$ ($\alpha = x, y$). Here \tilde{U}_0 denotes the strength of the effective attraction and $f_{\alpha, \mathbf{k}}$ represents the form factor of the p_α -wave pairing.

Then the chiral p-wave gap function $\Delta_{\mathbf{k}} = \Delta_x \sin k_x + \Delta_y \sin k_y$ is determined self-consistently with initial values $(\Delta_x, \Delta_y) = (1, i)\Delta_0$. The self-consistent expression is given by:

$$\Delta_{\mathbf{k}}(\mathbf{q}, T) = \frac{1}{N} \sum_{\mathbf{k}'} \tilde{U}_{\mathbf{k}, \mathbf{k}'} \langle \hat{c}_{-\mathbf{k}'+\mathbf{q}} \hat{c}_{\mathbf{k}'+\mathbf{q}} \rangle \quad (3)$$

where N is the number of unit cells, and $\langle \dots \rangle$ denotes the expectation value in the ground state. By utilizing Eq. (3), we are able to examine how the amplitude of the order parameter, denoted as Δ_x and Δ_y , varies with

temperature and supercurrent. The expression for these variations is determined by:

$$\Delta_\alpha(\mathbf{q}, T) = \frac{1}{N} \sum_{\mathbf{k}} \tilde{U}_\alpha f_\alpha \langle \hat{c}_{-\mathbf{k}+\mathbf{q}} \hat{c}_{\mathbf{k}+\mathbf{q}} \rangle \quad (4)$$

Here, $f_\alpha = \sin k_\alpha$ for p_α -wave pairing, and we set $\tilde{U}_x = \tilde{U}_y = \tilde{U}_0$. Different phases can be determined based on these variations.

Furthermore, the mean-field Hamiltonian is given by:

$$\hat{H} = \sum_{\mathbf{k}} \xi_{\mathbf{k}+\mathbf{q}} \hat{c}_{\mathbf{k}+\mathbf{q}}^\dagger \hat{c}_{\mathbf{k}+\mathbf{q}} + \sum_{\mathbf{k}} (\Delta_{\mathbf{k}} \hat{c}_{\mathbf{k}+\mathbf{q}}^\dagger \hat{c}_{-\mathbf{k}+\mathbf{q}}^\dagger + \text{h.c.}) + \frac{N|\Delta_{\mathbf{k}}|^2}{\tilde{U}_0} \quad (5)$$

and it can be also expressed by a matrix in the Nambu basis $\Psi_{\mathbf{k}} = (\hat{c}_{\mathbf{k}+\mathbf{q}}, \hat{c}_{-\mathbf{k}+\mathbf{q}}^\dagger)^t$ as follows:

$$\mathcal{H}_{\mathbf{k}}(\mathbf{q}) = \begin{pmatrix} \xi_{\mathbf{k}+\mathbf{q}} & \Delta_{\mathbf{k}} \\ \Delta_{\mathbf{k}}^* & -\xi_{\mathbf{k}-\mathbf{q}} \end{pmatrix} \quad (6)$$

Hence, the quasiparticle energy can be derived from the Hamiltonian as:

$$E_{\mathbf{k},\pm}(\mathbf{q}) = \frac{1}{2}(\xi_{\mathbf{k}+\mathbf{q}} - \xi_{-\mathbf{k}+\mathbf{q}}) \pm \sqrt{\left[\frac{1}{2}(\xi_{\mathbf{k}+\mathbf{q}} + \xi_{-\mathbf{k}+\mathbf{q}}) \right]^2 + |\Delta_{\mathbf{k}}|^2} \quad (7)$$

At small \mathbf{q} , it can also be approximated as $E_{\mathbf{k},\pm}(\mathbf{q}) \simeq \mathbf{k} \cdot \mathbf{q}/m \pm \sqrt{\xi_{\mathbf{k}}^2 + |\Delta_{\mathbf{k}}|^2} \simeq \mathbf{v}_F \cdot \mathbf{q} \pm \sqrt{\xi_{\mathbf{k}}^2 + |\Delta_{\mathbf{k}}|^2}$. This dispersion includes a Doppler shift in the continuum limit [48], and it is no longer symmetric along $E = 0$ due to the presence of a supercurrent.

Through out the study, we do not take into account the screening effects in a charged superfluid. However, all of the major conclusions are expected to uphold qualitatively.

B. Phase diagram

To simplify notation, we take $\hbar = c = k_B = e = 1$. Through all calculations, we assume $t = 1$ and take the supercurrent to flow along x direction, $\mathbf{q} = (q_x, 0)$.

Figure 2 (a) and (b) shows a representative set of zero-temperature results for p_x -wave, p_y -wave and $p_x + ip_y$ pairings. One noteworthy feature is the distinct response of the order parameter in the single-component p_x and p_y -wave states to supercurrent. In particular, while the p_x -wave order parameter Δ_x barely changes with increasing q_x prior to a first order transition beyond which it vanishes, Δ_y varies more drastically as a function of q_x . This distinction can be attributed to the rather different supercurrent-induced correction

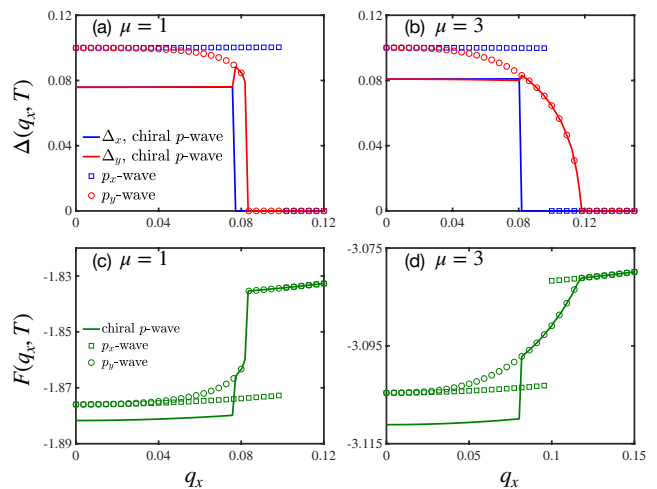


FIG. 2. The variation of self-consistent order parameters (upper panel) and free energy (lower panel) as a function of q_x at zero temperature. The energy reference is chosen to be $t = 1$. The left and right panels show results for different chemical potentials $\mu = 1$ and $\mu = 3$. In each case the strength of the pairing interaction \tilde{U}_0 is chosen such that the self-consistent pairing amplitude $\Delta_0 = 0.1$ in the pure p_x - or p_y -wave states. These calculations are performed in the \mathbf{k} -space with a size of $N = 1000 \times 1000$.

to the quasiparticle spectrum, which happens in conjunction with the different nodal position of the individual gap functions [34]. The p_x pairing has its nodal points at $\mathbf{k} = (0, \pm k_F)$, hence the Doppler shift at the nodal momenta is $\delta E_{\mathbf{k}} \approx \mathbf{k} \cdot \mathbf{q}/m = 0$. For p_y pairing, the nodal points are located at $\mathbf{k} = (\pm k_F, 0)$, hence $\delta E_{\mathbf{k}} \approx k_F q_x/m$. At the special chemical potential $\mu = 0$ in our particle-hole symmetric square lattice model, the four nodal momenta of p_x and p_y pairings coincide. We have checked that the two order parameters vary in very much similar fashion in that special case. The above behavior of Δ_x and Δ_y does not necessarily carry over to the two-component $p_x + ip_y$ calculations at finite temperature, due to the change of gap structure. For example, at $T > 0$ and small q_x , Δ_x in the $p_x + ip_y$ state could change more rapidly than Δ_y does as a function of q_x (Fig. 3 (a)), unlike in the single-component calculations (Fig. 3 (b)).

In the presence of a supercurrent, it is not known a priori whether chiral p-wave will be energetically more favorable than the nonchiral single-component p_x -wave and p_y -wave pairings. Furthermore, it is unclear whether self-consistent iterations with an initial chiral p-wave pairing can return the correct lowest energy state at large supercurrent. This can be seen in Fig. 2 (a) and (b). On the one hand, the relative robustness of single-component p_x (Δ_x) and p_y (Δ_y) pairings against supercurrent varies with model detail, i.e. chemical potential: at $\mu = 1$, Δ_x persists to stronger supercurrent, and it is the other way around at $\mu = 3$. On the other hand, in chiral p-wave cal-

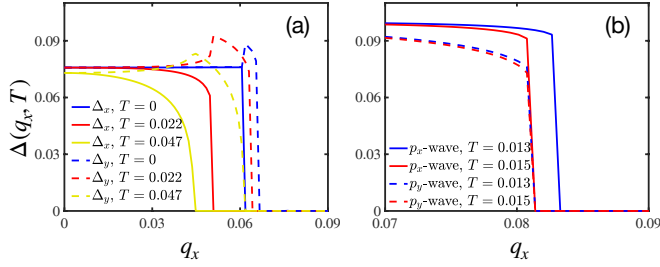


FIG. 3. The evolution of self-consistent order parameters as a function of q_x at finite temperature for different models (a) $p_x + ip_y$ and (b) $p_{x/y}$ -wave with chemical potential $\mu = 1$. The parameters are the same as in Fig. 2 (a).

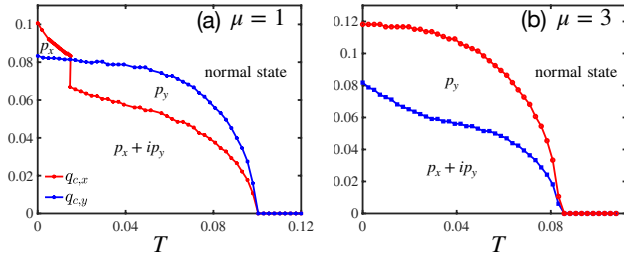


FIG. 4. The q - T phase diagram of chiral p-wave models with different chemical potential (a) $\mu = 1$ and (b) $\mu = 3$. Parameters are the same as in Fig. 2.

culations, Δ_y in general seems to survive up to stronger supercurrent than Δ_x does. Hence self-consistent calculations with initial chiral p-wave condition may in some circumstances obtain states that are not lowest energy, as exemplified in Fig. 2 (c). We thus consider all three different initial conditions, and compare their final self-consistent free energy $F(q_x, T) = \langle H \rangle$ to determine the phase diagram. The q_x - T phase diagrams of the above calculations are shown in Fig. 4. At finite q_x , the two order parameter components generically onsets at different temperatures. In most regime, Δ_y is more robust against supercurrent and calculation with initial chiral p-wave condition can obtain correct results. However, due to the above-mentioned subtle dependence on microscopic parameters, in the case of $\mu = 1$ and at low temperatures and large q_x , Δ_x becomes more robust (Fig. 4 (a)).

C. Specific heat

At intermediate supercurrent, both order parameter components are finite at zero temperature and their transitions split (e.g. Fig. 5 (a)). In principle, the onset of the secondary order parameter component shall manifest as a change in the superfluid density or the magnetic penetration depth, which can be detected by scanning SQUID experiments [26]. The second transition shall also naturally emerge as a specific heat anomaly,

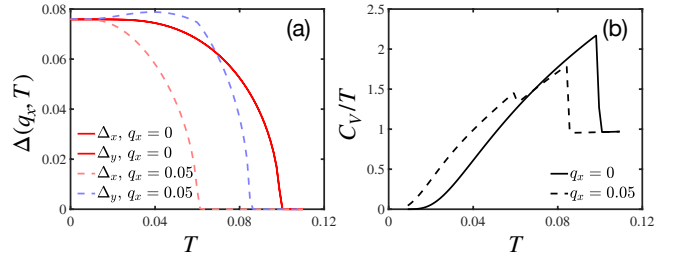


FIG. 5. The evolution of self-consistent order parameters (a) and the specific heat (b) as functions of temperature in the chiral p-wave model with $\mu = 1$, considering different supercurrent momenta. Parameters are the same as in Fig. 2.

as we numerically verify in this section. We evaluate the specific heat according to the thermodynamic relation $C_V(T) = T\partial S(T)/\partial T$. Here, $S(T)$ represents the temperature-dependent entropy of the system, which can be derived from the partition function as follows:

$$S(T) = -\frac{\partial G}{\partial T}, \quad G = -T \ln \text{tr}(e^{-\beta \hat{H}}) \quad (8)$$

Given the Hamiltonian Eq. (5), the definition Eq. (8) yields the following expression for $S(\mathbf{q}, T)$:

$$\begin{aligned} S(\mathbf{q}, T) &= - \sum_{\mathbf{k}, \zeta = \pm} \{ [1 - f(E_{\mathbf{k}, \zeta}(\mathbf{q}))] \ln(1 - f(E_{\mathbf{k}, \zeta}(\mathbf{q}))) \\ &\quad + f(E_{\mathbf{k}, \zeta}(\mathbf{q})) \ln f(E_{\mathbf{k}, \zeta}(\mathbf{q})) \} \end{aligned} \quad (9)$$

where $f(E) = 1/(e^{\beta E} + 1)$ denotes the Fermi-Dirac distribution function and $E_{\mathbf{k}, \pm}(\mathbf{q})$ has been defined in Eq. (7). Figure 5 (b) presents the temperature dependence of the specific heat for scenarios without and with supercurrent. In the latter scenario, a smaller but genuine anomaly emerges at the onset temperature of the secondary superconducting component shown in Fig. 5 (a).

In practice, specific heat measurement of a sample in a setup with externally applied current may be challenging. In particular, as the sample is thermally connected to external heat source via the electrodes through which the external current is applied, heat exchange near the electrode contacts cannot be circumvented. It is thus necessary to minimize the thermal contact by using, for example, thin and long gold or platinum wires for the electrodes. In addition, above the superconducting transition, the resistive sample is also heated on its own by the application of external current. To avoid this complication, it is better to perform the measurement from low to high temperatures. An alternative approach which can avoid the thermal contact issue is by using ring-shape samples. In this setup, supercurrent can be induced by threading a flux through the ring.

D. Edge modes

The topologically non-trivial $p_x + ip_y$ state supports gapless chiral edge modes at the boundaries. This section focuses on how these edge modes are affected under the influence of the supercurrent. To analyze the behavior of the edge modes, we first take a continuum model and solve for the edge states at an open boundary parallel to x -axis. In this geometry, the y -component of the wavevectors are no longer good quantum numbers. Making the substitution $k_y \rightarrow -i\partial_y$, the Hamiltonian given in Eq. (6) becomes

$$\begin{pmatrix} \frac{1}{2m} [(k_x + q_x)^2 - \partial_y^2] - \mu & \frac{\Delta_x}{k_F} k_x + \frac{\Delta_y}{k_F} \partial_y \\ \frac{\Delta_x}{k_F} k_x - \frac{\Delta_y}{k_F} \partial_y & -\frac{1}{2m} [(k_x - q_x)^2 - \partial_y^2] + \mu \end{pmatrix} \quad (10)$$

In the case of small supercurrent, i.e. $q_x/m \ll v_F$, we can simplify the Hamiltonian by neglecting the second-order term q_x^2 . This allows us to rewrite the Hamiltonian as two distinct parts:

$$\mathcal{H}_{k_x}(q_x) = \mathcal{H}_{1,k_x} + \frac{k_x}{m} q_x \sigma_0 \quad \text{with} \quad (11)$$

$$\mathcal{H}_{1,k_x} = \left[\frac{1}{2m} (k_x^2 - \partial_y^2) - \mu \right] \sigma_3 + \frac{\Delta_x}{k_F} k_x \sigma_1 + \frac{i\Delta_y}{k_F} \partial_y \sigma_2 \quad (12)$$

where σ_μ denotes the Pauli matrix.

We note that \mathcal{H}_{1,k_x} remains independent of q_x and represents the original Hamiltonian without supercurrent, whose solutions of edge modes are well-documented in previous literature. The chiral edge dispersion is given by

$$E_{\text{edge},k_x}(q_x = 0) = \frac{\Delta_x}{k_F} k_x \quad (13)$$

These states propagate unidirectionally at the boundary. For the time-reversed $p_x - ip_y$ state, the above dispersion acquires a minus sign and the propagation also switches direction. At finite q_x , we see from Eq. (11) that the slope of the edge dispersion is changed by q_x/m ,

$$E_{\text{edge},k_x}(q_x) = \left(\frac{\Delta_x}{k_F} + \frac{q_x}{m} \right) k_x \quad (14)$$

Reversing the supercurrent leads to an opposite change of slope, as depicted in the right panel of Fig. 1.

To verify the above semiclassical analysis, we perform numerical simulation of our square lattice model in a stripe geometry, with open boundaries in the y -direction and periodic boundary condition in the x -direction. For

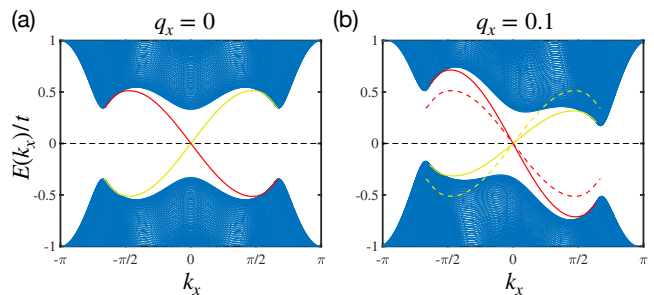


FIG. 6. Dispersion of chiral p-wave models along x direction with (a) $q_x = 0$ and (b) $q_x = 0.1$. The red and green solid lines represent the chiral edge dispersions at opposite edges. And in panel (b), the red and green dashed lines depict the chiral edge mode dispersions for the case when $q_x = 0$. Parameters: $(\Delta_x, \Delta_y, \mu) = (0.4, 0.4, 1)t$.

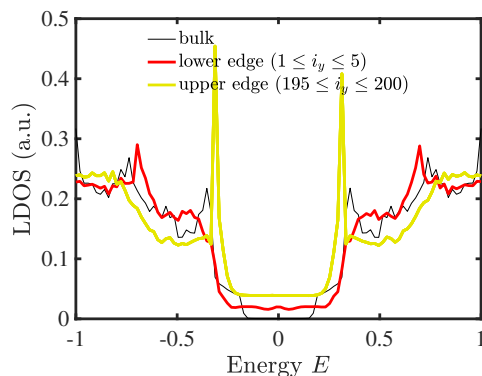


FIG. 7. The averaged LDOS of five sites near two opposite edges in the presence of a supercurrent with $q_x = 0.1$. The lower edge and upper edge are illustrated in Fig. 1 along the y -axis, and it is noteworthy that these two edges experience opposite supercurrents. The system consists of $N_y = 200$ lattice sites in the y direction, and the parameters used are the same as in Fig. 6 (b).

each supercurrent q_x , the Hamiltonian can be written as

$$\begin{aligned} \hat{H} = & \sum_{k_x, i_y} [2t \cos(k_x + q_x) - \mu] \hat{c}_{k_x, i_y}^\dagger \hat{c}_{k_x + q_x, i_y} \\ & + \sum_{k_x, i_y} (t \hat{c}_{k_x + q_x, i_y + 1}^\dagger \hat{c}_{k_x + q_x, i_y} + \text{h.c.}) \\ & + \sum_{k_x, i_y} (\Delta_x \sin k_x \hat{c}_{k_x + q_x, i_y}^\dagger \hat{c}_{-k_x + q_x, i_y}^\dagger \\ & + \Delta_y \hat{c}_{k_x + q_x, i_y + 1}^\dagger \hat{c}_{-k_x + q_x, i_y}^\dagger \\ & - \Delta_y \hat{c}_{k_x + q_x, i_y - 1}^\dagger \hat{c}_{-k_x + q_x, i_y}^\dagger + \text{h.c.}) \end{aligned} \quad (15)$$

Figure 6 compares the low energy spectrum of the above model for zero and finite q_x . As the chiral edge modes at the two open boundaries propagate in opposite direction, the supercurrent alters the slope of the two edge dispersions in opposite manner (Fig. 6 (b)), which is consistent with the above semiclassical expectation. Note that sig-

natures of edge modes in Sr_2RuO_4 have been reported in some tunneling spectroscopic studies [49, 50], although those data cannot confirm whether the pairing is chiral in nature.

The peculiar response of chiral edge modes to opposite supercurrents naturally manifests as distinct changes in the tunneling spectrum. Figure 7 shows the local density of states averaged over multiple sites in the vicinity of the two edges in the presence of a supercurrent. Note that the lower edge result is equivalent to the upper edge one with opposite supercurrent. The difference is noticeable. This could provide a diagnosis for the chiral pairing, possibly more efficient than the experimental attempts to probe the spontaneous chiral edge current. This is because the spontaneous current in real samples could be rather small, hence the related magnetic field could potentially be too weak to register a signal in actual experiments.

III. SUMMARY AND FURTHER REMARKS

In this study, we proposed to probe the possible chiral superconductivity in Sr_2RuO_4 and other materials through the application of a supercurrent. Akin to the effect of in-plane uniaxial strains and in-plane magnetic fields, supercurrent generically lifts the degeneracy of the two chiral superconducting order parameter components, giving rise to two superconducting transitions with observable thermodynamic and magnetic signatures. Moreover, opposite supercurrents incur distinct modifications to the unidirectionally propagating chiral edge modes and their tunneling spectra. We discussed possible measurements to detect these supercurrent-induced changes.

Note that our calculations have not accounted for the magnetic flux nor vortices generated by the supercurrent. Nonetheless, the conclusions are expected to hold even when those physics are considered. For example, while vortices drifting in supercurrent may give rise to fluctuating edge tunneling spectrum, the time-averaged spectra obtained under opposite supercurrents will likely still show discernible difference. We also take note of the stable tunneling spectra obtained in a conventional superconductor subject to a bias supercurrent [33]. Our study shall also apply to the chiral $d_{xz} + id_{yz}$ state and the nonunitary mixed helical p-wave pairings [51]. The latter essentially consists of two copies of chiral p-wave pairing with opposite chirality and unequal gap amplitudes (thus referred to as chiral-like states).

However, the presence of subgap edge modes and spontaneous edge current is not unique to chiral or chiral-like superconducting states. The same boundary phe-

nomenology, including the supercurrent induced effects discussed above, may also occur at certain boundaries of nonchiral but TRSB states. For example, they can appear in an $s + id_{xy}$ state on a square lattice at edges parallel to the x - or y -direction, but not at edges parallel to diagonals of the lattice [52]. Thus the dependence on edge orientation may help to distinguish chiral and nonchiral TRSB states, in addition to the polar Kerr effect measurement.

Finally, while the crystal structure of Sr_2RuO_4 respects inversion symmetry, possibility of mixed parity superconducting states has been raised [53]. Such states are formed by coexisting odd- and even-parity order parameters Δ_e and Δ_o . When the two order parameters condense with a phase difference of $\pm\pi/2$, the resultant state breaks both time-reversal and spatial inversion symmetries but preserves the product of the two. Since supercurrent is also invariant under the joint operation of time-reversal and spatial inversion, it couples to a composite order parameter as follows,

$$iJ(\Delta_e^*\Delta_o - \Delta_o^*\Delta_e) \quad (16)$$

Two nontrivial consequences ensue. Firstly, for a specific TRSB state, such as $(\Delta_e, \Delta_o) = (|\Delta_e|, i|\Delta_o|)$, the above coupling contributes opposite free energies for opposite supercurrents. This reflects a nonreciprocal response of the system to supercurrent. Observable features would include a number of nonlinear optical effects [54–56], as well as the so-called superconducting diode effect featuring unequal critical currents in opposite directions [57]. Secondly, in contrast to Eq. (1), the above coupling introduces a linear enhancement of the superconducting transition temperature, similar to the linear cusping behavior expected for a chiral $p_x + ip_y$ or $d_{xz} + id_{yz}$ state under uniaxial strains.

IV. ACKNOWLEDGEMENTS

We acknowledge many helpful comments and suggestions by Prof. Ying Liu. This work is supported by NSFC under grant No. 11904155, the Guangdong Provincial Key Laboratory under Grant No. 2019B121203002, the Guangdong Science and Technology Department under Grant 2022A1515011948, a Shenzhen Science and Technology Program (Grant No. KQTD20200820113010023), and the Pingshan District Innovation Platform Project of Shenzhen Hi-tech Zone Development Special Plan in 2022 (Grant No. 29853M-KCJ-2023-002-01). Computing resources are provided by the Center for Computational Science and Engineering at Southern University of Science and Technology.

[1] G. M. Luke, Y. Fudamoto, K. M. Kojima, M. I. Larkin, J. Merrin, B. Nachumi, Y. J. Uemura, Y. Maeno, Z. Q.

Mao, Y. Mori, H. Nakamura, and M. Sigrist. *Nature* **394**, 558–561 (1998).

- [2] J. Xia, Y. Maeno, P. T. Beyersdorf, M. M. Fejer, and A. Kapitulnik, *Phys. Rev. Lett.* **97**, 167002 (2006).
- [3] G. M. Luke, A. Keren, L. P. Le, W. D. Wu, Y. J. Uemura, D. A. Bonn, L. Taillefer, and J. D. Garrett. *Phys. Rev. Lett.* **71**, 1466 (1993).
- [4] E. R. Schemm, W. J. Gannon, C. M. Wishne, W. P. Halperin, and A. Kapitulnik. *Science* **345**, 190-193(2014).
- [5] D. E. MacLaughlin, D. W. Cooke, R. H. Heffner, R. L. Hutson, M. W. McElfresh, M. E. Schillaci, H. D. Rempp, J. L. Smith, J. O. Willis, E. Zirngiebl, C. Boekema, R. L. Lichti, and J. Oostens. *Phys. Rev. B* **37**, 3153 (1988).
- [6] E. R. Schemm, R. E. Baumbach, P. H. Tobash, F. Ronning, E. D. Bauer, and A. Kapitulnik. *Phys. Rev. B* **91**, 140506(R) (2015).
- [7] Y. Maeno, H. Hashimoto, K. Yoshida, S. Nishizaki, T. Fujita, J. G. Bednorz, F. Lichtenberg, *Nature (London)* **372**, 532 (1994).
- [8] Y. Maeno, T. M. Rice, and M. Sgrist, *Phys. Today* **54** (1), 42 (2001).
- [9] A. P. Mackenzie and Y. Maeno. *Rev. Mod. Phys.* **75**, 657 (2003).
- [10] C. Kallin and A. J. Berlinsky. *J. Phys.: Condens. Matter* **21**, 164210 (2009).
- [11] C. Kallin. *Rep. Prog. Phys.* **75** 042501 (2012).
- [12] Y. Maeno, S. Kittaka, T. Nomura, S. Yonezawa, and K. Ishida, *J. Phys. Soc. Jpn.* **81**, 011009 (2012).
- [13] Y. Liu and Z. Q. Mao, *Physica C: Superconductivity and its Application*, **514**, 339 (2015).
- [14] C. Kallin and J. Berlinsky, *Rep. Prog. Phys.* **79**, 054502 (2016).
- [15] A. P. Mackenzie, T. Scaffidi, C. W. Hicks and Y. Maeno. *npj Quant Mater* **2**, 40 (2017).
- [16] W. Huang, *Chin. Phys. B*, **30**, 107403 (2021).
- [17] A. J. Leggett, Y. Liu, *J Supercond Nov Magn* **34**, 1647-1673 (2021).
- [18] K. Ishida, H. Mukuda, Y. Kitaoka, K. Asayama, Z. Q. Mao, Y. Mori and Y. Maeno. *Nature* **396**, 658-660 (1998).
- [19] J. A. Duffy, S. M. Hayden, Y. Maeno, Z. Mao, J. Kulda, and G. J. McIntyre, *Phys. Rev. Lett.* **85**, 5412 (2000).
- [20] K. D. Nelson, Z. Q. Mao, Y. Maeno, Y. Liu. *Science* **306**, 1151-1154(2004).
- [21] A. Pustogow, Yongkang Luo, A. Chronister, Y.-S. Su, D. A. Sokolov, F. Jerzembeck, A. P. Mackenzie, C. W. Hicks, N. Kikugawa, S. Raghu, E. D. Bauer and S. E. Brown. *Nature* **574**, 72-75 (2019).
- [22] A. Chronister, A. Pustogow, N. Kikugawa, D. A. Sokolov, F. Jerzembeck, C. W. Hicks, A. P. Mackenzie, E. D. Bauer, and S. E. Brown, *Proc. Natl. Acad. Sci. (USA)* **118**, e2025313118 (2021).
- [23] M. Sgrist and K. Ueda. *Rev. Mod. Phys.* **63**, 239-311 (1991).
- [24] V. Grinenko, S. Ghosh, R. Sarkar, J.-C. Orain, A. Nikitin, M. Elender, D. Das, Z. Guguchia, F. Brückner, M. E. Barber, J. Park, N. Kikugawa, D. A. Sokolov, J. S. Bobowski, T. Miyoshi, Y. Maeno, A. P. Mackenzie, H. Luetkens, C. W. Hicks, and H.-H. Klauss. *Nat. Phys.* **17**, 748-754 (2021).
- [25] Y.-S. Li, N. Kikugawa, D. A. Sokolov, F. Jerzembeck, A. S. Gibbs, Y. Maeno, C. W. Hicks, J. Schmalian, M. Nicklas, and A. P. Mackenzie. *Proc. Natl. Acad. Sci. USA* **118**, e2020492118 (2021).
- [26] E. Mueller, Y. Iguchi, C. Watson, C. Hicks, Y. Maeno, K. Moler, *arXiv:2306.13737*.
- [27] C. W. Hicks, D. O. Brodsky, E. A. Yelland, A. S. Gibbs, J. A. N. Bruin, M. E. Barber, S. D. Edkins, K. Nishimura, S. Yonezawa, Y. Maeno, and A. P. Mackenzie, *Science* **344**, 283-285 (2014).
- [28] A. Steppke, L. Zhao, M.E. Barber, T. Scaffidi, F. Jerzembeck, H. Bosner, A. S. Gibbs, Y. Maeno, S. H. Simon, A. P. Mackenzie and C. W. Hicks, *Science* **355**, eaaf9398 (2017).
- [29] C. A. Watson, A. S. Gibbs, A. P. Mackenzie, C. W. Hicks, and K. A. Moler. *Phys. Rev. B* **98**, 094521 (2018).
- [30] D.F. Agterberg. *Phys. Rev. Lett.* **80**, 5184 (1998).
- [31] R.P. Kaur, D.F. Agterberg, H. Kusunose. *Phys. Rev. B* **72**, 144528 (2005).
- [32] S. Yonezawa, T. Kajikawa, and Y. Maeno, *J. Phys. Soc. Jpn.* **83**, 083706 (2014).
- [33] A. Anthore, H. Pothier, and D. Esteve, *Phys. Rev. Lett.* **90**, 127001 (2003).
- [34] D. Zhang, C. S. Ting, and C.-R. Hu, *Phys. Rev. B* **70**, 172508 (2004).
- [35] P. Fulde and R. A. Ferrell. *Phys. Rev.* **135**, A550 (1964).
- [36] M. Stone and R. Roy. *Phys. Rev. B* **69**, 184511 (2004).
- [37] W. Huang, S. Lederer, E. Taylor, and C. Kallin. *Phys. Rev. B* **91**, 09450 (2015).
- [38] Y. Tada. *Phys. Rev. B* **92**, 104502 (2015).
- [39] Y. Imai, K. Wakabayashi, and M. Sgrist, *Phys. Rev. B* **85**, 174532 (2012); **88**, 144503 (2013).
- [40] W. Huang, E. Taylor, and C. Kallin, *Phys. Rev. B* **90**, 224519 (2014).
- [41] S. Lederer, W. Huang, E. Taylor, S. Raghu, and C. Kallin, *Phys. Rev. B* **90**, 134521 (2014).
- [42] T. Scaffidi and S. H. Simon, *Phys. Rev. Lett.* **115**, 087003 (2015).
- [43] Y. Tada, W. Nie, and M. Oshikawa, *Phys. Rev. Lett.* **114**, 195301 (2015).
- [44] J. R. Kirtley, C. Kallin, C. W. Hicks, E.-A. Kim, Y. Liu, K. A. Moler, Y. Maeno, and K. D. Nelson, *Phys. Rev. B* **76**, 014526 (2007).
- [45] C. W. Hicks, J. R. Kirtley, T. M. Lippman, N. C. Koshnick, M. E. Huber, Y. Maeno, W. M. Yuhasz, M. B. Maple, and K. A. Moler, *Phys. Rev. B* **81**, 214501 (2010).
- [46] P. J. Curran, S. J. Bending, W. M. Desoky, A. S. Gibbs, S. L. Lee, and A. P. Mackenzie, *Phys. Rev. B* **89**, 144504 (2014).
- [47] M. Tinkham, Introduction to Superconductivity. 2nd Edition, Dover Publication, Mineola, New York, 2004.
- [48] G. E. Volovik, *JETP Lett.* **58**, 469 (1993).
- [49] S. Kashiwaya, H. Kashiwaya, H. Kambara, T. Furuta, H. Yaguchi, Y. Tanaka, and Y. Maeno, *Phys. Rev. Lett.* **107**, 077003 (2011).
- [50] Yiqun Alex Ying's dissertation in physics at the Pennsylvania State University, 2012.
- [51] W. Huang and Z. Wang, *Phys. Rev. Res.* **3**, L042002 (2021).
- [52] A. Furusaki, M. Matsumoto, and M. Sgrist, *Phys. Rev. B* **64**, 054514 (2001).
- [53] T. Scaffidi, *Phys. Rev. B* **107**, 014505 (2023).
- [54] R. Wakatsuki, Yu Saito, S. Hoshino, Y. M. Itahashi, T. Ideue, M. Ezawa, Y. Iwasa, N. Nagaosa, *Sci. Adv.* **3**, e1602390 (2017).
- [55] R. WakatsuKi and N. Nagaosa, *Phys. Rev. Lett.* **121**, 026601 (2018).

- [56] Y. Tokura and N. Nagaosa, *Nat. Commun.* **9**, 3740 (2018).
- [57] F. Ando, Y. Miyasaka, T. Li, J. Ishizuka, T. Arakawa, Y. Shiotani, T. Moriyama, Y. Yanase, T. Ono, *Nature* **584**, 373 (2020).